arXiv:1110.1804v1 [cs.CV] 9 Oct 2011

The proximal point method for a hybrid model in image restoration

Zhi-Feng Pang[†,‡], Li-Lian Wang[‡], and Yu-Fei Yang[§]

Abstract Models including two L^1 -norm terms have been widely used in image restoration. In this paper we first propose the alternating direction method of multipliers (ADMM) to solve this class of models. Based on ADMM, we then propose the proximal point method (PPM), which is more efficient than ADMM. Following the operator theory, we also give the convergence analysis of the proposed methods. Furthermore, we use the proposed methods to solve a class of hybrid models combining the ROF model with the LLT model. Some numerical results demonstrate the viability and efficiency of the proposed methods.

Keywords: Image restoration; Alternating direction method of multipliers; Proximal point method; ROF model; LLT model; Hybrid model.

1. Introduction

Image restoration is of momentous significance in coherent imaging systems and various image processing applications. The goal is to recover the real image from the deteriorated image, e.g., image denoising, image deblurring and image inpainting, etc., see [5, 16, 38] for details.

For the additive noisy image, many denoising models have been proposed based on PDEs or variational methods over the last decades [5, 16, 38]. The essential idea for this class of models is to filter out the noise in an image while the significant features such as edges and textures are preserved. However, due to the ill-posed for the restoration problems, we have to employ some regularization methods [22] to overcome it. The general form of regularization methods consists in minimizing an energy functional of the following form

$$F(\bar{u}) = \frac{\lambda}{2}\|\bar{u} - \bar{u}_0\|_X^2 + \mathcal{R}(\bar{u}) \tag{1.1}$$

in Banach space X, where λ is the regularization parameter, $\mathcal{R}$ is a regularization term, $\bar{u}_0$ is the observed image and $\bar{u}$ is the image to be restored. The development of the energy functional (1.1) actually profits from the ROF model [42] which is of the following form

$$\min_{\bar{u}} \frac{\lambda_1}{2}\|\bar{u} - \bar{u}_0\|_{L^2(\Omega)}^2 + |\bar{u}|_{BV(\Omega)}, \tag{1.2}$$

where $BV(\Omega)$ is the space of functions of bounded variation defined on an open set Ω with Lipschitz boundary. Due to edge-preserving property of the term $|\bar{u}|_{BV(\Omega)}$, this model has been extended to other sorts of image processing problems such as

$$\min_{\bar{u}} \frac{\lambda_2}{2}\|K\bar{u} - \bar{u}_0\|_{L^2(\Omega)}^2 + |\bar{u}|_{BV(\Omega)} \tag{1.3}$$

[†]College of Mathematics and Information Science, Henan University, Kaifeng 475004, China.
[‡]Division of Mathematical Sciences, School of Physical and Mathematical Sciences, Nanyang Technological University, 637371, Singapore. E-mail: zhifengpang@163.com, lilian@ntu.edu.sg
[§]College of Mathematics and Econometrics, Hunan University, Changsha, 410082, China. E-mail:yfyang@hnu.edu.cn

*The research was supported in part by the NNSF of China (No. 60872129, 60835004) and.

for image deblurring [40] and

$$\min_{\bar{u}} \frac{\lambda_3}{2}\|\bar{u}-\bar{u}_0\|^2_{L^2(\Omega\setminus D)} + |\bar{u}|_{BV(\Omega)} \tag{1.4}$$

for image inpainting [16, 17], where K is a blurring operator and D is the inpainting domain. Furthermore, this model was applied to restore the multiplicative noisy image which usually appears in various image processing applications such as in laser images, ultrasound images [46], synthetic aperture radar (SAR) [4] and medical ultrasonic images [36]. One of models based on the space bounded variation space was proposed by Huang et al. (HNW) [29] with the form

$$\min_{z} \alpha \int_{\Omega} \left(z + fe^{-z}\right) \mathrm{d}x + |z|_{BV(\Omega)}, \tag{1.5}$$

where z is the logarithmic transformation of u and $|z|_{BV(\Omega)}$ keeps the total variation property related to $|e^z|_{BV(\Omega)}$ and $\alpha > 0$. Here u satisfies $f = u\eta$ for the noise η.

However, as we all know that the $|\cdot|_{BV(\Omega)}$ term usually reduces the computational solution of the above models to be piecewise constant, which is also called the staircasing effect in smooth regions of the image. The staircase effect implies to produce new edges that do not exist in the true image so that the restored image is unsatisfactory to the eye. To overcome this drawback, some high-order models have been proposed by replacing the $BV(\Omega)$ in the above models with $BV^2(\Omega)$ [15, 32, 43, 48] such as a model proposed by Lysaker, Lundervold, and Tai (the LLT model) with the following form

$$\min_{\bar{u}} \frac{\beta_1}{2}\|\bar{u}-\bar{u}_0\|^2_{L^2(\Omega)} + |\bar{u}|_{BV^2(\Omega)}. \tag{1.6}$$

However, there are some drawbacks for $BV^2(\Omega)$, e.g., this space can blur the edges of the image in the course of restoration. Therefore, it is a natural choice to combine the advantages of the ROF model and the LLT model if we want to preserve edges while avoiding the staircase effect in smooth regions. One of convex combinations between the $BV(\Omega)$ and $BV^2(\Omega)$ was proposed by Lysaker and Tai [32] to restore the image with additive noise. But their model is not quite intuitive due to lack of gradient information in the weighting function. Since the edge detector function $g(u_0) = \frac{1}{1+\varrho(\nabla(u_0 * G_\sigma(x))|}$ can depict the information of edges, we can employ it as a balance function, i.e., we can apply the following model

$$\min_{u} \frac{\beta}{2}\|u-\bar{u}_0\|^2_{L^2(\Omega)} + |u|_{BV_{(1-g)}(\Omega)} + |u|_{BV^2_g(\Omega)} \tag{1.7}$$

to restore the noisy image [31]. Here $G_\sigma(x)$ is the Gaussian kernel with the standard deviation σ and $\beta > 0$. Obviously, $|u|_{BV_{(1-g)}(\Omega)}$ tends to be predominant where edges most likely appear and $|u|_{BV^2_g(\Omega)}$ tends to be predominant at the locations with smooth signals. Based on the advantages of the hybrid model (1.7), we also extend it to the image restoration models (1.3)-(1.5) in this paper.

Another topic for image restoration is to find some efficient methods to solve the above proposed models. In fact, there are many different methods based on PDE or convex optimization to solve the minimization problem (1.1) by means of the specific models (1.2)-(1.6). For example, for the purpose of solving the ROF model (1.2) or the LLT model (1.6), we can use the gradient descent method [32, 42], the Chambolle's dual method [12, 13, 32], the primal and dual method [14, 24, 49], the second cone programming method [27], the multigrid method [20], operator splitting method [11, 28, 35] and the inverse scale method [10], etc. However, different from the ROF model (1.2) and the LLT model (1.6), the above proposed model (1.7) includes two L^1-norm

terms which make it more difficult to find some efficient numerical methods. In this paper, we mainly develop a proximal point method (PPM) to solve the proposed model (1.7), which can be actually fell into solving the following general framework

$$\min_u \frac{\theta}{2}\|u-f\|^2_{L^2(\Omega)} + h_1(\Lambda_1 u) + h_2(\Lambda_2 u), \tag{1.8}$$

where $h_1, h_2 : X \to R$ are proper, convex and lower semicontinuous (l.s.c.), Λ_1 and Λ_2 are bounded linear operators, θ is a parameter. A specific form of (1.8) was considered by Afonso et al. in [1] where the authors proposed a Bregman iterative method to solve the model with the combination of the L^1-norm term and the total variation (TV) term. It is obvious that the model (1.8) can be looked at as more general problems than this mentioned form. Simultaneously, we also give some facts to show that the proposed proximal point method can be deduced from the alternating direction augmented Lagrangian method (ADALM), which is based on the connection between the projection operator and the shrinkage operator. Furthermore, this proposed proximal point method not only keeps the advantages of the alternating direction augmented Lagrangian method (ADALM) but also requires much less computational cost. The convergence analysis of the proposed methods are given. Moreover, based on the proximal point method, we also extend the model (1.7) to image deblurring, image inpainting and the multiplicative noisy image restoration. Experimental results show that the restored images generated by the proposed models and methods are desirable.

The paper is organized as follows. In Section 2, we recall some knowledge related to functional spaces and convex analysis. In Section 3, we first proposed a the alternating direction augmented Lagrangian method (ADALM) to solve the problem (1.8) and then give the proximal point method (PPM) to improve this method. It is based on the correction between the proximal point operator and the shrinkage operator. In Section 4, we give some applications by using the proposed algorithms and also compare the related models and the proposed methods. Some concluding remarks are given in Section 5.

2. Functional spaces and convex analysis

In image processing problem based on PDEs or the variational methods, the functional spaces play an important role such as the bounded variation space, G-norm space and Besov space, c.f. [5, 34], etc. Furthermore, to easily get the related solutions, we usually consider the corresponding minimization energy functionals in the sense of convexity. In this section we first give some definitions and properties of $BV_g(\Omega)$ and $BV_g^2(\Omega)$, which are actually similar to those of $BV(\Omega)$ in [2, 3, 25]. Then we recall some concepts and useful properties of convex analysis [30].

2.1. Functional spaces

The bounded variation functional and the bounded Hessian functional spaces have played an important role in image restoration, e.g., image denoising and deblurring [5, 16, 41, 32, 40], image inpainting [18], image zooming [26] and image super-resolution [33], etc. In the following we give their definitions and some related results.

Definition 2.1. *Let $\Omega \in R^n$ be an open subset with Lipschitz boundary. $BV_g^i(\Omega)$ is defined as a subspace of $L^1(\Omega)$ with*

$$|v|_{BV_g^i(\Omega)} = \sup\{\int_\Omega g(x)v(x)\mathrm{div}^i\xi(x)\mathrm{dx} \mid \xi \in C_c^i(\Omega), |\xi|_{L^1(\Omega)} \le 1\} < \infty, \tag{2.1}$$

for some functional $g(x)$ which are independent to $v(x)$, where i=1 or 2. Especially, when i=1, we can omit it for simplicity.

It should be noticed that when g = 1 as a constant, the above functional spaces will be simplified as the usual functional spaces $BV(\Omega)$ and $BV^2(\Omega)$. As a sequence, we can deduce the following results, see [5, 16, 32, 41] for details.

Lemma 2.1. *Let Ω be an open subset of R^n with Lipschitz boundary and i=1 or 2, then the following assertions hold.*

(1) If $\{v_k\} \subseteq BV_g^i(\Omega)$ satisfies

$$\lim_{k\to\infty} \int_\Omega |v_k - v| \mathrm{dxdy} = 0,$$

or let $p > 1$ and $\{v_k\} \subseteq BV_g^i(\Omega)$ with $v_k \rightharpoonup v$ in $L^p(\Omega)$, then

$$|v|_{BV_g^i(\Omega)} \leq \liminf_{k\to\infty} |v_k|_{BV_g^i(\Omega)}.$$

Moreover, if

$$\liminf_{k\to\infty} |v_k|_{BV_g^i(\Omega)} < \infty$$

holds, then $v \in BV_g^i(\Omega)$.

(2) Let $\{v_k\} \in BV_g^i(\Omega)$, then there exists a sequence $v_k \in W^{i,1}(\Omega) \cap C^\infty(\Omega)$ such that

$$\lim_{k\to\infty} \int_\Omega |v_k - v| dxdy = 0 \text{ and } |v_k|_{BV_g^i(\Omega)} \to |v|_{BV_g^i(\Omega)}.$$

(3) $BV_g^i(\Omega)$ endowed with the norm

$$\|v\|_{BV_g^i}(\Omega) = |v|_{L^1(\Omega)} + \int_\Omega |D_g^i v| \mathrm{dx}$$

is a Banach space.

(4) If $v \in L^1(\Omega)$ satisfies $\|v\|_{L^1(\Omega)} + |v|_{BV_g^i(\Omega)} < \infty$ or $v \in L^2(\Omega)$ satisfies $\|v\|_{L^2(\Omega)} + |v|_{BV_g^i(\Omega)} < \infty$, then $v \in BV_g^i(\Omega)$.

(5) $v \in BV_g^2(\Omega)$ if and only if $v \in BV_g(\Omega)$ and $\frac{\partial v}{\partial x_j} \in BV_g(\Omega)$ for $j = \{1, 2, \cdots, n\}$. In particular

$$|v|_{BV_g^2(\Omega)} \leq \sum_{j=1}^n \left| \frac{\partial v_j}{\partial x_j} \right|_{BV_g(\Omega)} \leq n|v|_{BV_g^2(\Omega)}.$$

2.2. Convex analysis

Since many models with the form (1.1) are convex, we review some basic concepts and properties of convex analysis from the work of Ekeland and Teman [30] in this subsection. In fact, the convexity of the related models means that we can easily get the solution of (1.2) by employing some numerical methods. Here we assume that X and Y are the adjoint Banach space.

Definition 2.2. *Let $G : X \to R$ be a convex function. The subdifferential of G at a point $y \in X$ is defined by*

$$\partial G(y) = \{\eta : G(y) - G(x) \leq (\eta, y - x), \forall\, x \in X\},$$

where $\eta \in \partial G(y)$ is called a subgradient.

The subdifferential $\partial G(y)$ can be thought of as the set of hyperplanes passing through the point y which are less than $G(y)$, which will reduce to the classical gradient if $G(x)$ is differentiable. Furthermore, we have

$$G(x^*) = \min_{x \in X} G(x) \text{ if and only if } 0 \in \partial G(x^*), \tag{2.2}$$

where the right hand side of (2.2) is called the Euler-Lagrange equation of the minimization functional $G(x)$. On the other hand, if set $A = \partial G$, then A is a convex function. Furthermore, if assume that $G(x)$ is proper, then A is a maximal monotone operator. That is to say, if A is monotone which satisfies

$$(y_1 - y_2, x_1 - x_2) \geq 0$$

for all $y_1 \in A(x_1)$ and $y_2 \in A(x_2)$, A is maximal if it is not strictly contained in any other monotone operator on X. Given any positive scalar c, we call

$$J_{cA} = (I + cA)^{-1}$$

the resolvent of A. It is obvious that J_{cA} is a contraction defined on X for $c > 0$. Denote by H_c its Yosida approximation:

$$H_{cA} = \frac{1}{c}(I - J_{cA}),$$

where I denotes the identity operator [8, 6]. For the resolvent J_{cA} and the Yosida approximation H_{cA}, we have the following result.

Lemma 2.2. *Set $x_1, x_2 \in X$ and A is a maximal monotone operator, then the operators H_{cA} and J_{cA} satisfy*

$$\frac{1}{c^2}\|J_{cA}(x_1) - J_{cA}(x_2)\|_{L^2}^2 + \|H_{cA}(x_1) - H_{cA}(x_2)\|_{L^2}^2 \leq \frac{1}{c^2}\|x_1 - x_2\|_{L^2}^2.$$

Proof. Let x_i (i=1,2) be solutions of

$$x_i \in y_i + cA(y_i),$$

then we can obtain

$$\begin{aligned} \|x_1 - x_2\|_{L^2}^2 &= \|y_1 - y_2 + c(A(y_1) - A(y_2))\|_{L^2}^2 \\ &= \|y_1 - y_2\|_{L^2}^2 + c^2\|A(y_1) - A(y_2)\|_{L^2}^2 + 2c(y_1 - y_2, A(y_1) - A(y_2)) \\ &\geq \|y_1 - y_2\|_{L^2}^2 + c^2\|A(y_1) - A(y_2)\|_{L^2}^2 \\ &= \|J_{cA}x_1 - J_{cA}x_2\|_{L^2}^2 + c^2\|H_{cA}(x_1) - H_{cA}(x_2)\|_{L^2}^2, \end{aligned}$$

which implies that the assertion holds. □

We now give some useful properties about the primal function and the conjugate function [30].

Definition 2.3. *Let $G : X \to R$ be a convex proper function. The conjugate function of G is defined by*

$$G^*(x^*) = \sup_{x \in X}\{(x, x^*) - G(x)\}$$

for $\forall\, x^* \in X$.

Lemma 2.3. *For the conjugate function G^* of G, the following assertions hold.*

(1) The function G^* is convex and lower semicontinuous.

(2) $x^* \in \partial G(x)$ if and only if

$$G(x) + G(x^*) = (x, x^*).$$

(3) $x^* \in \partial G(x)$ if and only if $x \in \partial G^*(x^*)$.

Definition 2.4. *Let $G : X \to R$ be convex and $t > 0$. The proximal mapping to $G : X \to Y$ is defined by*

$$Prox_t G(x) := \arg\min_y \{G(y) + \frac{1}{2t}\|y - x\|_{L^2}^2\} \tag{2.3}$$

for $y \in X$.

It is well known that the above mapping is called the Moreau proximal mapping [19]. The minimizer of the optimization problem (2.3) exists and is unique when the function $G(y)$ is convex and proper, which also makes this optimization problem well-posed. On the other hand, if set $A(y) = \partial G(y)$, we can find that

$$y = Prox_t G(x) \Longleftrightarrow y = J_{tA}(x).$$

Furthermore, based on Lemma 2.2, we can get the following results for the proximal point operator $Prox_t G(x)$.

Corollary 2.1. *For any $x_1, x_2 \in X$, the proximal operator is firmly nonexpansive, i.e., $Prox_t G(x)$ satisfies*

$$\|Prox_t G(x_1) - Prox_t G(x_2)\|_{L^2}^2 + \|(x_1 - Prox_t G(x_1)) - (x_2 - Prox_t G(x_2)\|_{L^2}^2 \leq \|x_1 - x_2\|_{L^2}^2.$$

Theorem 2.1. *Assume that $G : X \to R$ and G^* is the conjugate function of G. Then the following result*

$$Prox_t G(x) + Prox_{\frac{1}{t}} G^*(x) = x, \tag{2.4}$$

holds for $t > 0$.

Proof. Following the definition of the proximal mapping to $G(x)$ in (2.3) and the Euler-Lagrange equation of the problem (2.2), we have

$$0 \in \partial G(Prox_t G(x)) + \frac{1}{t}(Prox_t G(x) - x),$$

which can be reformulated as

$$\frac{1}{t}(x - Prox_t G(x)) \in \partial G(Prox_t G(x)). \tag{2.5}$$

Therefore, based on the third property of Lemma 2.3, the formula (2.5) can be written as

$$tProx_t G(x) \in \partial G^*(x - Prox_t G(x)),$$

which naturally follows that

$$0 \in \partial G^*(x - Prox_t(G(x)) + t(x - Prox_t G(x) - x).$$

Using Definition 2.4 again, we can deduce that

$$x - Prox_t G(x) = Prox_{\frac{1}{t}} G^*(x),$$

which implies that the assertion holds. □

Definition 2.5. *The projection operator* $\mathcal{P}_{\mathcal{B}_\tau}(\cdot) : X \to Y$ *onto the closed disc* $\mathcal{B}_\tau := \{x \in X : |x|_{L^1} \leq \frac{1}{\tau}\}$ *is defined by*

$$\mathcal{P}_{\mathcal{B}_\tau}(x) = \frac{x}{|x|_{L^1}} \min(|x|_{L^1}, \frac{1}{\tau}),$$

where $x \in X$ *and* $\tau > 0$.

Definition 2.6. *The shrinkage operator* $S_\tau(\cdot) : X \to Y$ *is defined by*

$$\mathcal{S}_\tau(x) = \frac{x}{|x|_{L^1}} \max\Big(|x|_{L^1} - \frac{1}{\tau}, 0\Big),$$

where we use the convention $\frac{0}{0} = 0$.

In fact, it is easy to find that the projection operator $\mathcal{P}_{\mathcal{B}_\tau}(x)$ can be looked at as the solution of

$$\min_y \frac{1}{2}\|y - x\|_{L^2}^2 + \delta(y),$$

where the characteristic function $\delta(y)$ satisfies

$$\delta(y) = \begin{cases} 0, & \text{if } y \in \mathcal{B}, \\ \infty, & \text{if } y \notin \mathcal{B} \end{cases} \tag{2.6}$$

and the shrinkage operator $S_\tau(x)$ is the solution of

$$\min_y \frac{\tau}{2}\|y - x\|_{L^2}^2 + |y|_{L^1}.$$

Furthermore, we also notice that if set $E_D(x) = |x|_{L^1}$, the conjugate function of $E_P(x)$ is then equal to $\delta(x) := E_D(x)$. On the other hand, $E_P(x)$ is the conjugate function of $E_D(x)$ which follows that $E_P(x)$ is proper and convex. So we can get the following result based on Theorem 2.1.

Corollary 2.2. *The projection operator* $\mathcal{P}_{\mathcal{B}_\tau}(\cdot)$ *and the shrinkage operator* $S_\tau(\cdot)$ *satisfy*

$$\mathcal{P}_{\mathcal{B}_\tau}(x) + S_\tau(x) = x$$

for any $x \in X$.

3. The alternating direction method of multipliers (ADMM) and the proximal point method (PPM)

Variable splitting methods such as the alternating direction method of multipliers (ADMM) [45, 47] and the operator splitting methods [30, 33, 44] have been recently used in the image restoration problem. The key of this class of methods is to transform the original problem into some subproblems so that we can easily solve these subproblems by employing some numerical methods. In this section we first consider to use the alternating direction method of multipliers (ADMM) to solve the general minimization problem (1.8). However, ADMM has a loose form so that the computational complexity is tediously increased. In order to overcome this drawback,

we thus change this method to a compact form called the proximal method based on Corollary 2.2.

3.1. The alternating direction method of multipliers (ADMM)

We consider the following constrained problem

$$\begin{aligned} &\min_{u,v,w} \frac{\theta}{2}\|u-f\|_{L^2}^2 + h_1(v) + h_2(z), \\ &\text{s.t. } v = \Lambda_1 u,\ z = \Lambda_2 u, \end{aligned} \tag{3.1}$$

which is clearly equivalent to the constrained problem (1.8) in the feasible set $\{(u,v,z) : v = \Lambda_1 u, \text{ and } z = \Lambda_2 u\}$. Throughout the following subsections, we always assume that Λ_1 and Λ_2 are a surjective map. It seems that the problem (3.1) including three variables looks more complex than the original unconstrained problem (1.8). In fact, this problem can be solved more easily under the condition that h_1 and h_2 are nondifferentiable. In the augmented Lagrangian framework [9], the problem (3.1) equivalently solves the following minimization Lagrangian function

$$\begin{aligned} \min_{u,v,z,\zeta_1,\zeta_2,\mu_1,\mu_2} L(u,v,z,\zeta_1,\zeta_2,\mu_1,\mu_2) \quad = \quad & \frac{\theta}{2}\|u-f\|_{L^2}^2 + h_1(v) + (\zeta_1, \Lambda_1 u - v) + \frac{\mu_1}{2}\|\Lambda_1 u - v\|_{L^2}^2 \\ & + h_2(z) + (\zeta_2, \Lambda_2 u - z) + \frac{\mu_2}{2}\|\Lambda_2 u - z\|_{L^2}^2, \end{aligned} \tag{3.2}$$

where ζ_i is the Lagrangian multiplier and μ_i is the penalty parameter for $i = 1, 2$. Then we can use the following augmented Lagrangian method (ALM)

$$\begin{cases} (u^n, v^n, z^n) = \arg\min_{u,v,z} L(u,v,z,\zeta_1^{n-1},\zeta_2^{n-1},\mu_1,\mu_2) & \text{(3.3a)} \\ \zeta_1^n = \zeta_1^{n-1} + \mu_1(\Lambda_1 u - v) & \text{(3.3b)} \\ \zeta_2^n = \zeta_2^{n-1} + \mu_2(\Lambda_2 u - z) & \text{(3.3c)} \end{cases}$$

with choosing the original values ζ_0^1 and ζ_0^2 to solve (3.2). If set $d_i^n = \frac{\zeta_i^n}{\mu_i}$ for $i = 1, 2$ and omit the terms which are independent of (u^n, v^n, z^n) in (3.3a), the above strategy (3.3) can be written as

$$\begin{cases} (u^n, v^n, z^n) = \arg\min_{u,v,z} \frac{\theta}{2}\|u-f\|_{L^2}^2 + h_1(v) + \frac{\mu_1}{2}\|\Lambda_1 u - v + d_1^{n-1}\|_{L^2}^2 + h_2(z) \\ \qquad\qquad + \frac{\mu_2}{2}\|\Lambda_2 u - z + d_2^{n-1}\|_{L^2}^2 & \text{(3.4a)} \\ d_1^n = d_1^{n-1} + \Lambda_1 u^n - v^n & \text{(3.4b)} \\ d_2^n = d_2^{n-1} + \Lambda_2 u^n - z^n & \text{(3.4c)} \end{cases}$$

for the original values d_0^1 and d_2^0. Then we can use the following so-called alternating direction method of multipliers (ADMM) to solve (3.4).

Algorithm 3.1. *Alternating direction method of multipliers (ADMM) for solving (3.4).*

(1) Choose the original values: v^0, z^0, d_1^0 and d_2^0. Set $\theta, \mu_1, \mu_2 > 0$ and $n = 1$;

(2) Compute $(u^n, v^n, z^n, d_1^n, d_2^n)$ by

$$\begin{cases} u^n = \arg\min\limits_u \underbrace{\dfrac{\theta}{2}\|u-f\|_{L^2}^2 + \dfrac{\mu_1}{2}\|\Lambda_1 u - v^{n-1} + d_1^{n-1}\|_{L^2}^2 + \dfrac{\mu_2}{2}\|\Lambda_2 u - z^{n-1} + d_2^{n-1}\|_{L^2}^2}_{=h(u)}, & (3.5a)\\ v^n = \arg\min\limits_v h_1(v) + \dfrac{\mu_1}{2}\|\Lambda_1 u^n - v + d_1^{n-1}\|_{L^2}^2, & (3.5b)\\ z^n = \arg\min\limits_z h_2(z) + \dfrac{\mu_2}{2}\|\Lambda_2 u^n - z + d_2^{n-1}\|_{L^2}^2, & (3.5c)\\ d_1^n = d_1^{n-1} + \Lambda_1 u^n - v^n, & (3.5d)\\ d_2^n = d_2^{n-1} + \Lambda_2 u^n - z^n; & (3.5e) \end{cases}$$

(3) If the stop criterion is not satisfied, set $n := n+1$ and go to the step (2).

Since $h(u)$ is differentiable and strictly convex, we can get the unique solution of (3.5a) which satisfies

$$\begin{cases} \theta(u^n - f) + \mu_1\Lambda_1^*(\Lambda_1 u^n - v^{n-1} + d_1^{n-1}) + \mu_2\Lambda_2^*(\Lambda_2 u^n - z^{n-1} + d_2^{n-1}) = 0, & (3.6a)\\ 0 \in w_1^n + \mu_1(v^n - d_1^{n-1} - \Lambda_1 u^n), & (3.6b)\\ 0 \in w_2^n + \mu_2(z^n - d_2^{n-1} - \Lambda_2 u^n), & (3.6c)\\ d_1^n = d_1^{n-1} + \Lambda_1 u^n - v^n, & (3.6d)\\ d_2^n = d_2^{n-1} + \Lambda_2 u^n - z^n, & (3.6e) \end{cases}$$

where Λ_1^* and Λ_2^* are the adjoint operators of Λ_1 and Λ_2, respectively. It follows that the solution u^n in (3.6a) can be directly gotten by the following explicit formulation

$$u^n = \underbrace{(\theta I + \mu_1\Lambda_1^*\Lambda_1 + \mu_2\Lambda_2^*\Lambda_2)}_{M}^{-1}(\theta f + \mu_1\Lambda_1^*(v^{n-1} - d_1^{n-1}) + \mu_2\Lambda_2^*(z^{n-1} - d_2^{n-1}))$$

However, when the operator M is ill-posed, the solution is unsuitable or unavailable. Hence we have to go back to (3.6a) and to employ some iteration strategy such as the Gauss-Seidel method to solve this equation. On the other hand, it is obvious that (3.5b) and (3.5c) can be looked at as the proximal mapping, so the solutions of the minimization problems (3.5b) and (3.5c) can be obviously written as

$$v^n = Prox_{\frac{1}{\mu_1}h_1}(\Lambda_1 u^n + d_1^{n-1}) \text{ and } z^n = Prox_{\frac{1}{\mu_2}h_2}(\Lambda_2 u^n + d_2^{n-1}). \tag{3.7}$$

Theorem 3.1. *Assume that $(u^*, v^*, z^*, w_1^*, w_2^*)$ is the saddle point of the Lagrange function*

$$\mathcal{L}(u, v, z, w_1, w_2) = \frac{\theta}{2}\|u-f\|_{L^2}^2 + h_1(v) + (w_1, \Lambda_1 u - v) + h_2(z) + (w_2, \Lambda_2 u - z). \tag{3.8}$$

Then (u^*, v^*, z^*) is the solution of (3.5) and the sequence $\{(u^n, v^n, z^n)\}$ generated by Algorithm 3.1 converges to this solution. Furthermore, u^* is also the solution of the minimization problem (1.8).

Proof. Following the assumption, we can find that the saddle point $(u^*, v^*, z^*, w_1^*, w_2^*)$ of (3.8) satisfies

$$\begin{cases} 0 = \theta(u^* - f) + \Lambda_1^* w_1^* + \Lambda_2^* w_2^*,\\ 0 \in p_1^* - w_1^*,\\ 0 \in p_2^* - w_2^*,\\ 0 = \Lambda_1 u^* - v^*,\\ 0 = \Lambda_2 u^* - z^* \end{cases} \tag{3.9}$$

with $p_1^* \in \partial h_1(v^*)$ and $p_2^* \in \partial h_2(z^*)$. If set $d_1^* = \frac{w_1^*}{\mu_1}$ and $d_2^* = \frac{w_2^*}{\mu_2}$, then (3.9) can be written as

$$\begin{cases} 0 = \theta(u^* - f) + \mu_1\Lambda_1^*(\Lambda_1 u^* - v^* + d_1^*) + \mu_2\Lambda_2^*(\Lambda_2 u^* - z^* + d_2^*), & (3.10a)\\ 0 \in w_1^* + \mu_1(v^* - d_1^* - \Lambda_1 u^*), & (3.10b)\\ 0 \in w_2^* + \mu_2(z^* - d_2^* - \Lambda_2 u^*), & (3.10c)\\ d_1^* = d_1^* + \Lambda_1 u^* - v^*, & (3.10d)\\ d_2^* = d_2^* + \Lambda_2 u^* - z^*, & (3.10e) \end{cases}$$

which implies that $(u^*, v^*, z^*, w_1^*, w_2^*)$ is the solution of (3.5). Furthermore, the above equations (3.10) can be rewritten as a compact form

$$0 \in \theta(u^* - f) + \Lambda_1^*\partial h_1(\Lambda_1 u^*) + \Lambda_2^*\partial h_2(\Lambda_2 u^*),$$

which also implies that u^* is the solution of the minimization problem (1.8).

Set

$$u_e^n = u^n - u^*, v_e^n = v^n - v^*, z_e^n = z^n - z^*, d_{1e}^n = d_1^n - d_1^*, d_{2e}^n = d_2^n - d_2^*$$

denote the related errors. Then subtracting (3.6) by (3.10) and using the similar strategy as did in [11], we successively obtain

$$\begin{cases} 0 = \theta\|u_e^n\|_{L^2}^2 + \mu_1\|\Lambda_1 u_e^n\|_{L^2}^2 + \mu_2\|\Lambda_2 u_e^n\|_{L^2}^2 - \mu_1(v_e^{n-1} - d_{1e}^{n-1}, \Lambda_1 u_e^n) - \mu_2(z_e^{n-1} - d_{2e}^{n-1}, \Lambda_2 u_e^n),\\ 0 = \mu_1\|v_e^n\|_{L^2}^2 + \mu_1(v_e^n, d_{1e}^n - d_{1e}^{n-1} - \Lambda_1 u_e^n),\\ 0 = \mu_2\|z_e^n\|_{L^2}^2 + \mu_2(z_e^n, d_{2e}^n - d_{2e}^{n-1} - \Lambda_2 u_e^n),\\ 0 = \mu_1\|d_{1e}^n\|_{L^2}^2 - \mu_1\|d_{1e}^{n-1}\|_{L^2}^2 + 2\mu_1(d_{1e}^{n-1}, v_e^n - \Lambda_1 u_e^n) - \mu_1\|v_e^n - \Lambda_1 u_e^n\|_{L^2}^2,\\ 0 = \mu_2\|d_{2e}^n\|_{L^2}^2 - \mu_2\|d_{2e}^{n-1}\|_{L^2}^2 + 2\mu_2(d_{2e}^{n-1}, z_e^n - \Lambda_2 u_e^n) - \mu_2\|z_e^n - \Lambda_2 u_e^n\|_{L^2}^2, \end{cases}$$

where $d_{1e}^n \in \frac{1}{\mu_1}\partial h_1(v_{1e}^n)$ and $d_{2e}^n \in \frac{1}{\mu_2}\partial h_2(z_{1e}^n)$. Summing the above five equations, we get

$$\begin{aligned} &\frac{\mu_1}{2}(\|d_{1e}^{n-1}\|_{L^2}^2 - \|d_{1e}^n\|_{L^2}^2) + \frac{\mu_2}{2}(\|d_{2e}^{n-1}\|_{L^2}^2 - \|d_{2e}^n\|_{L^2}^2)\\ &= \theta\|u_e^n\|_{L^2}^2 + \mu_1\Big[(d_{1e}^n, v_e^n) + \frac{1}{2}\|\Lambda_1 u_e^n - v_e^{n-1}\|_{L^2}^2 + \frac{1}{2}\|v_e^n\|_{L^2}^2 - \frac{1}{2}\|v_e^{n-1}\|_{L^2}^2\Big]\\ &+\mu_2\Big[(d_{2e}^n, z_e^n) + \frac{1}{2}\|\Lambda_2 u_e^n - z_e^{n-1}\|_{L^2}^2 + \frac{1}{2}\|z_e^n\|_{L^2}^2 - \frac{1}{2}\|z_e^{n-1}\|_{L^2}^2\Big]. \end{aligned}$$

So it is easy to deduce that

$$\begin{aligned} &\frac{\mu_1}{2}\Big[\|d_{1e}^1\|_{L^2}^2 - \|d_{1e}^N\|_{L^2}^2) + \frac{\mu_2}{2}(\|d_{2e}^1\|_{L^2}^2 - \|d_{2e}^N\|_{L^2}^2\Big]\\ &= \sum_{n=1}^{N}\Big[\theta\|u_e^n\|_{L^2}^2 + \mu_1(d_{1e}^n, v_e^n) + \frac{\mu_1}{2}\|\Lambda_1 u_e^n - v_e^{n-1}\|_{L^2}^2 + \mu_2(d_{2e}^n, z_e^n)\\ &+\frac{\mu_2}{2}\|\Lambda_2 u_e^n - z_e^{n-1}\|_{L^2}^2\Big] + \frac{\mu_1}{2}\|v_e^N\|_{L^2}^2 - \frac{\mu_1}{2}\|v_e^1\|_{L^2}^2 + \frac{\mu_2}{2}\|z_e^N\|_{L^2}^2 - \frac{\mu_2}{2}\|z_e^1\|_{L^2}^2. \end{aligned} \quad (3.11)$$

Following the fact that $h(x)$ is strictly convex, $d_{1e}^n \in \frac{1}{\mu}\partial h_1(v_e^n)$ and $d_{2e}^n \in \frac{1}{\mu}\partial h_2(z_e^n)$, we can get

$$(d_{1e}^n, v_e^n) \geq 0 \text{ and } (d_{2e}^n, z_e^n) \geq 0.$$

Combined with(3.11), it follows that

$$\sum_{n=1}^{N}\|u_e^n\|_{L^2}^2 < \infty, \ \sum_{n=1}^{N}\|\Lambda_1 u_e^n - v_e^{n-1}\|_{L^2}^2 < \infty \text{ and } \sum_{n=1}^{N}\|\Lambda_2 u_e^n - z_e^{n-1}\|_{L^2}^2 < \infty.$$

Then we deduce that

$$\lim_{n\to\infty} u^n = u^*$$

and

$$\lim_{n\to\infty} \|\Lambda_1 u_e^n - v_e^{n-1}\|_{L^2}^2 = 0 \text{ and } \lim_{n\to\infty} \|\Lambda_2 u_e^n - z_e^{n-1}\|_{L^2}^2 = 0.$$

So we have

$$\lim_{n\to\infty} \|v^n - v^*\|_{L^2}^2 = 0 \text{ and } \lim_{n\to\infty} \|z^n - z^*\|_{L^2}^2 = 0.$$

Hence the proof is complete. □

Notice that Algorithm 3.1 can be actually looked at as the split Bregman method [28]. The based idea of this method is to introduce some intermediate variables so as to transform the original problem into some subproblems which are easily solved. The connection between the split Bregman method and the alternating direction method of multipliers (ADMM) has been shown in [23, 45]. However, our algorithm consider the sum of three convex functions, which is more general than the related algorithms in [23, 28].

3.2. The proximal point method

Though the alternating direction method of multipliers (ADMM) can effectively solve the original problem (3.1), this method actually suffers from a looser form as did in [28, 33], which can badly affect its efficiency. In this subsection, based on Theorem 2.1, we propose a proximal point method (PPM), which has a compacter form compare so that it can improve the efficiency of the ADMM. Now we rewritten (3.5) with a little variation as the following form:

$$\begin{cases} v^n = \arg\min_v h_1(v) + \dfrac{\mu_1}{2}\|v - d_1^{n-1} - \Lambda_1 u^{n-1}\|_{L^2}^2, & (3.12a)\\ z^n = \arg\min_z h_2(z) + \dfrac{\mu_2}{2}\|z - d_2^{n-1} - \Lambda_2 u^{n-1}\|_{L^2}^2, & (3.12b)\\ d_1^n = d_1^{n-1} + \Lambda_1 u^{n-1} - v^n, & (3.12c)\\ d_2^n = d_2^{n-1} + \Lambda_2 u^{n-1} - z^n, & (3.12d)\\ u^n = \arg\min_u \dfrac{\theta}{2}\|u - f\|_{L^2}^2 + \dfrac{\mu_1}{2}\|\Lambda_1 u - v^n + d_1^n\|_{L^2}^2 + \dfrac{\mu_2}{2}\|\Lambda_2 u - z^n + d_2^n\|_{L^2}^2 & (3.12e) \end{cases}$$

with the first order optimality conditions given by

$$\begin{cases} v^n = prox_{\frac{1}{\mu_1}} h_1(\Lambda_1 u^{n-1} + d_1^{n-1}), & (3.13a)\\ z^n = prox_{\frac{1}{\mu_1}} h_2(\Lambda_2 u^{n-1} + d_2^{n-1}), & (3.13b)\\ d_1^n = d_1^{n-1} + \Lambda_1 u^{n-1} - v^n, & (3.13c)\\ d_2^n = d_2^{n-1} + \Lambda_2 u^{n-1} - z^n, & (3.13d)\\ \theta(u^n - f) + \mu_1\Lambda_1^*(\Lambda_1 u^n - v^n + d_1^n) + \mu_2\Lambda_2^*(\Lambda_2 u^n - z^n + d_2^n) = 0. & (3.13e) \end{cases}$$

If (3.13e) is replaced by

$$\theta(u^n - f) + \mu_1\Lambda_1^*(\Lambda_1 u^{n-1} - v^n + d_1^{n-1}) + \mu_2\Lambda_2^*(\Lambda_2 u^{n-1} - z^n + d_2^{n-1}) = 0,$$

it follows from (3.13) and Theorem 3.1 that

$$\begin{cases} d_1^n = prox_{\mu_1} h_1^*(\Lambda_1 u^{n-1} + d_1^{n-1}) \\ d_2^n = prox_{\mu_2} h_2^*(\Lambda_2 u^{n-1} + d_2^{n-1}), \\ u^n = f - (\frac{\mu_1}{\theta}\Lambda_1^* d_1^n + \frac{\mu_2}{\theta}\Lambda_2^* d_2^n). \end{cases} \tag{3.14}$$

So we propose the following algorithm to solve (3.1).

Algorithm 3.2. *Proximal point method (PPM) for solving (3.1).*

(1) Choose the original value d_1^1, d_2^1 and u^1. Set $\mu_1, \mu_2 > 0$ and $n = 1$;

(2) Compute (d_1^n, d_2^n, u^n) by (3.14).

(3) If the stop criterion is not satisfied, set $n := n + 1$ and go to the step (2).

Theorem 3.2. *Assume that $h_1(x)$ and $h_2(u)$ are convex and proper. If $\mu_1 \in (0, \frac{1}{\theta\|\Lambda_1\|^2})$ and $\mu_2 \in (0, \frac{1}{\theta\|\Lambda_2\|^2})$, here $\|\cdot\| := \max\{\|Kx\|_{L^2} : x \in X \text{ with } \|x\|_{L^2} \le 1\}$ for a continuous linear operator K. Then the sequence $\{(u^n, d_1^n, d_2^n)\}$ generated by Algorithm 3.2 converges to the limit point $(\bar{d}_1, \bar{d}_2, \bar{u})$. Furthermore, the limit point $\bar{u}$ is the solution of (1.8).*

Proof. Set $A_1(x) := \partial h_1(x)$ and $A_2(x) := \partial h_2(x)$, then operators A_1 and A_2 are maximal monotone. Following from (3.13) and the definition of the Yosida approximation, (3.14) can be equivalently written as

$$\begin{cases} \mu_1 d_1^n = H_{\frac{A_1}{\mu_1}}(\Lambda_1 u^{n-1} + d_1^{n-1}), & \text{(3.15a)} \\ \mu_2 d_2^n = H_{\frac{A_2}{\mu_2}}(\Lambda_2 u^{n-1} + d_2^{n-1}), & \text{(3.15b)} \\ u^n = f - (\frac{\mu_1}{\theta}\Lambda_1^* d_1^n + \frac{\mu_2}{\theta}\Lambda_2^* d_2^n). & \text{(3.15c)} \end{cases}$$

Then, by (3.15) and Lemma 2.2, we can deduce that

$$\begin{aligned} &\|J_{\frac{A_1}{\mu_1}}(\Lambda_1\bar{u} + \bar{d}_1) - J_{\frac{A_1}{\mu_1}}(\Lambda_1 u^{n-1} + d_1^{n-1})\|_{L^2}^2 + \|\mu_1(\bar{d}_1 - d_1^n)\|_{L^2}^2 \\ &\qquad \le \|\Lambda_1(\bar{u} - u^{n-1}) + (\bar{d}_1 - d_1^{n-1})\|_{L^2}^2 \end{aligned} \tag{3.16}$$

and

$$\begin{aligned} &\|J_{\frac{A_2}{\mu_2}}(\Lambda_2\bar{u} + \bar{d}_2) - J_{\frac{A_2}{\mu_2}}(\Lambda_2 u^{n-1} + d_2^{n-1})\|_{L^2}^2 + \|\mu_2(\bar{d}_2 - d_2^n)\|_{L^2}^2 \\ &\qquad \le \|\Lambda_2(\bar{u} - u^{n-1}) + (\bar{d}_2 - d_2^{n-1})\|_{L^2}^2. \end{aligned} \tag{3.17}$$

Combining (3.16) and (3.17) with

$$\begin{aligned} &(\Lambda_1(\bar{u} - u^{n-1}), \mu_1(\bar{d}_1 - d_1^{n-1})) + (\Lambda_2(\bar{u} - u^{n-1}), \mu_2(\bar{d}_2 - d_2^{n-1})) = -\frac{1}{\theta}\|\bar{u} - u^{n-1}\|_{L^2}^2 \\ &\le -\frac{1}{2\theta\|\Lambda_1\|^2}\|\Lambda_1(\bar{u} - u^{n-1})\|_{L^2}^2 - \frac{1}{2\theta\|\Lambda_2\|^2}\|\Lambda_2(\bar{u} - u^{n-1})\|_{L^2}^2, \end{aligned}$$

which implies that

$$\begin{aligned} &\mu_1\|J_{\frac{A_1}{\mu_1}}(\Lambda_1\bar{u} + \bar{d}_1) - J_{\frac{A_1}{\mu_1}}(\Lambda_1 u^{n-1} + d_1^{n-1})\|_{L^2}^2 + \mu_1\|\mu_1(\bar{d}_1 - d_1^n)\|_{L^2}^2 + \mu_2\|J_{\frac{A_2}{\mu_2}}(\Lambda_2\bar{u} + \bar{d}_2) \\ &-J_{\frac{A_2}{\mu_2}}(\Lambda_2 u^{n-1} + d_2^{n-1})\|_{L^2}^2 + \mu_2\|\mu_2(\bar{d}_2 - d_2^n)\|_{L^2}^2 \\ &\le (\mu_1 - \frac{1}{\theta\|\Lambda_1\|^2})\|\Lambda_1(\bar{u} - u^{n-1})\|_{L^2}^2 + \mu_1\|\bar{d}_1 - d_1^{n-1}\|_{L^2}^2 + (\mu_2 - \frac{1}{\theta\|\Lambda_2\|^2})\|\Lambda_2(\bar{u} - u^{n-1})\|_{L^2}^2 \\ &+\mu_2\|\bar{d}_2 - d_2^{n-1}\|_{L^2}^2. \end{aligned} \tag{3.18}$$

Since $\mu_1 \leq \frac{1}{\theta\|\Lambda_1\|^2}$ and $\mu_2 \leq \frac{1}{\theta\|\Lambda_2\|^2}$, by (3.17) we eventually get

$$\|\bar{d}_1 - d_1^n\|_{L^2} \leq \|\bar{d}_1 - d_1^{n-1}\|_{L^2} \text{ and } \|\bar{d}_2 - d_2^n\|_{L^2} \leq \|\bar{d}_2 - d_2^{n-1}\|_{L^2}$$

as long as $u^n \neq \bar{u}$ and

$$\lim_{n\to\infty} \|u^{n-1} - \bar{u}\|_{L^2} = 0.$$

Furthermore, by (3.18) we also get

$$\lim_{n\to\infty} \|J_{\frac{A_1}{\mu_1}}(\Lambda_1\bar{u} + \bar{d}_1) - J_{\frac{A_1}{\mu_1}}(\Lambda_1 u^{n-1} + d_1^{n-1})\|_{L^2} = 0$$

and

$$\lim_{n\to\infty} \|J_{\frac{A_2}{\mu_2}}(\Lambda_1\bar{u} + \bar{d}_2) - J_{\frac{A_2}{\mu_2}}(\Lambda_2 u^{n-1} + d_2^{n-1})\|_{L^2} = 0.$$

Based on (3.15a) and (3.15b), using the definitions of resolvent and the Yosida approximation, it is easy to find that

$$\lim_{n\to\infty} \|d_1^n - d_1^{n-1}\|_{L^2} = 0 \text{ and } \lim_{n\to\infty} \|d_2^n - d_2^{n-1}\|_{L^2} = 0.$$

Then, using the Corollary 4 in P.199 of [39], we can deduce that $\lim_{n\to\infty} d_1^n = \bar{d}_1$ and $\lim_{n\to\infty} d_2^n = \bar{d}_2$.

On the other hand, if $(\bar{d}_1, \bar{d}_2, \bar{u})$ is the limit of the sequence $\{(d_1^n, d_2^n, u^n)\}$ generated by Algorithm 3.2, it is easy to find that (3.14) can be rewritten as

$$\begin{cases} \bar{d}_1 = prox_{\mu_1} h_1^*(\Lambda_1\bar{u} + \bar{d}_1) \\ \bar{d}_2 = prox_{\mu_2} h_2^*(\Lambda_2\bar{u} + \bar{d}_2) \\ \bar{u} = f - (\frac{\mu_1}{\theta}\Lambda_1^*\bar{d}_1 + \frac{\mu_2}{\theta}\Lambda_2^*\bar{d}_2) \end{cases}$$

as $n \to +\infty$. Using Theorem 2.1, (3.16) can be then rewritten as

$$\begin{cases} \Lambda_1\bar{u} = prox_{\frac{1}{\mu_1}} h_1(\Lambda_1\bar{u} + \bar{d}_1), & \text{(3.19a)} \\ \Lambda_2\bar{u} = prox_{\frac{1}{\mu_2}} h_2(\Lambda_2\bar{u} + \bar{d}_2), & \text{(3.19b)} \\ \bar{u} = f - (\frac{\mu_1}{\theta}\Lambda_1^*\bar{d}_1 + \frac{\mu_2}{\theta}\Lambda_2^*\bar{d}_2). & \text{(3.19c)} \end{cases}$$

Following from (3.19a) and (3.19b), we can find that

$$\begin{cases} \bar{d}_1 = \frac{1}{\mu_1}\partial h_1(\Lambda_1(\bar{u})), \\ \bar{d}_2 = \frac{1}{\mu_2}\partial h_2(\Lambda_2(\bar{u})), \end{cases} \tag{3.20}$$

Submitting (3.19) into (3.20), we have

$$\theta(\bar{u} - f) + \Lambda_1^*\partial h_1(\Lambda_1(\bar{u})) + \Lambda_2^*\partial h_2(\Lambda_2(\bar{u})) = 0,$$

which implies that $\bar{u}$ is the solution of (1.8). □

4. Some applications in image restoration

In Subsection 4.1, we apply the alternating direction method of multipliers (ADMM) and the above proximal point method (PPM) to the image denoising problem. Here we also compare the proposed hybrid model with the ROF model and the LLT model. Then, based on the proposed hybrid model, we set the PPM as a basic method to solve image deblurring, image inpainting and image denoising for the multiplicative noise in the last three subsections. For simplicity, we assume that the image region Ω is squared with the size $M\times M$ and set $S = R^{M\times M}$, $T = S\times S$ and $Z = T\times T$ as did in [12]. The usual scalar product can be denoted as $\langle u, v\rangle_S := \sum_{i=1}^{M} u_i v_i$ for $u, v \in S$, $\langle p^1, p^2\rangle_T := \sum_{i=1}^{M}\sum_{j=1}^{M} p^1_{i,j} p^2_{i,j}$ for $p^1, p^2 \in T$ and $(p, q)_Z = \sum_{i,j=1}^{M} (p^{11}_{i,j} q^{11}_{i,j} + p^{12}_{i,j} q^{12}_{i,j} + p^{21}_{i,j} q^{21}_{i,j} + p^{22}_{i,j} q^{22}_{i,j})$ for $p, q \in Z$. The L^1 norm of $p = (p_1, p_2) \in T$ is defined by $|p|_{L^1} = \sqrt{p_1^2 + p_2^2}$ and the L^1 norm of $q = (q_1, q_2; q_3, q_4) \in Z$ is defined by $|q|_{L^1} = \sqrt{q_1^2 + q_2^2 + q_3^2 + q_4^2}$. If $u \in S$, we use $\nabla^+ = (\nabla^+_x, \nabla^+_y) \in T$ to denote the first order forward difference operator with

$$\nabla^+_x u_{i,j} = \begin{cases} u_{i+1,j} - u_{i,j} & \text{for } 1 \le i < N \\ 0 & \text{for } i = N \end{cases} \quad \text{and } \nabla^+_y u_{i,j} = \begin{cases} u_{i,j+1} - u_{i,j} & \text{for } 1 \le j < N \\ 0 & \text{for } j = N \end{cases}$$

and use $\nabla^- = (\nabla^-_x, \nabla^-_y)$ to denote the first order backward difference operator with

$$\nabla^-_x u_{i,j} = \begin{cases} -u_{i,j}, & \text{for } i = 1 \\ u_{i,j} - u_{i-1,j} & \text{for } 1 < i < N \\ u(i,j) & \text{for } i = N \end{cases} \quad \text{and } \nabla^-_y u_{i,j} = \begin{cases} -u_{i,j} & \text{for } j = 1 \\ u_{i,j} - u_{i,j-1} & \text{for } 1 < j < N \\ u_{i,j} & \text{for } j = N \end{cases}$$

for $i, j = 1, \cdots, N$. Based on the first order difference operators, we can give the second order difference operator as follows

$$\nabla^2 u_{i,j} = \begin{pmatrix} \nabla^-_x(\nabla^+_x u_{i,j}) & \nabla^+_x(\nabla^+_y u_{i,j}) \\ \nabla^-_y(\nabla^-_x u_{i,j}) & \nabla^-_y(\nabla^+_y u_{i,j}) \end{pmatrix} \in Z.$$

Using the same approach, we can define some other second order operators such as $\nabla^+_x(\nabla^-_x u_{i,j})$, $\nabla^-_x(\nabla^-_y u_{i,j})$, $\nabla^+_y(\nabla^+_x u_{i,j})$ and $\nabla^+_y(\nabla^-_y u_{i,j})$. Then we can give the first order and the second divergence operators as

$$\begin{aligned} \mathrm{div} u_{i,j} &= \nabla^-_x u_{i,j} + \nabla^-_y u_{i,j}, \\ \mathrm{div}^2 u_{i,j} &= \nabla^+_x(\nabla^-_x u_{i,j}) + \nabla^-_x(\nabla^-_y u_{i,j}) + \nabla^+_y(\nabla^+_x u_{i,j}) + \nabla^+_y(\nabla^-_y u_{i,j}). \end{aligned}$$

Furthermore, if set $p \in T$ and $q \in Z$, it is easy to deduce that

$$\|\mathrm{div} p\|^2_S \le 8\|p\|^2_T \text{ and } \|\mathrm{div}^2 q\|^2_S \le 64\|q\|^2_Z. \tag{4.1}$$

Remark 4.1. *The related examples in the following subsections are performed using Windows 7 and Matlab 2009(a) on a desktop with Intel Core i5 processor at 2.4 GHz and 4 GB memory. All of the parameters for related models are chosen by trial and empirically which can yield better restored images. On the other hand, we should notice that it is not very expensive when we use the ADMM and the PPM to get u^n, but the total computational effort of one outer iteration requiring many inner steps can be very huge. In order to reduce the computational effort and keep fair comparison of these two methods, we so simplify the inner-outer iterative framework by performing only one-step in inner iteration. It is obvious that these sets are very efficient from the following numerical experiences.*

4.1. Image denoising for the additive noise

In this subsection, we consider to use the alternating direction method of multipliers (ADMM) and the proposed proximal point method (PPM) to solve (1.7) for restoring the additive noisy image. Following the definitions of $|u|_{BV_{(1-g)}}$ and $|u|_{BV_g^2}$, we can set $\Lambda_1 = \nabla$ and $\Lambda_2 = \nabla^2$, then the algorithms are proposed as follows.

Algorithm 4.1. *Alternating direction method of multipliers (ADMM) to solve (1.7).*

(1) Choose the original $d_1^0 = v^0 = \boldsymbol{0} \in T$ *and* $d_2^0 = z^0 = \boldsymbol{0} \in Z$. *Set* $\mu_1, \mu_2 > 0$ *and* $n = 1$;

(2) Compute $(u^n, v^n, z^n, d_1^n, d_2^n)$ *by*

$$\begin{cases} (\theta I - \mu_1 \triangle + \mu_2 \triangle^2) u^n = \theta f + \mu_1 \mathrm{div}(v^{n-1} - d_1^{n-1}) - \mu_2 \mathrm{div}^2(z^{n-1} - d_2^{n-1}) & (4.2a) \\ v^n = \dfrac{\nabla u^n + d_1^{n-1}}{|\nabla u^n + d_1^{n-1}|_{L^1}} \cdot \max(|\nabla u^n + d_1^{n-1}|_{L^1} - \dfrac{(1-g(x))}{\mu_1}, 0), & (4.2b) \\ z^n = \dfrac{\nabla^2 u^n + d_2^{n-1}}{|\nabla^2 u^n + d_2^{n-1}|_{L^1}} \cdot \max(|\nabla^2 u^n + d_2^{n-1}|_{L^1} - \dfrac{g(x)}{\mu_2}, 0), & (4.2c) \\ d_1^n = d_1^{n-1} + \nabla u^n - v^n, & (4.2d) \\ d_2^n = d_2^{n-1} + \nabla^2 u^n - z^n, & (4.2e) \end{cases}$$

where $\triangle = \mathrm{div} \circ \nabla$ *and* $\triangle^2 = \mathrm{div}^2 \circ \nabla^2$;

(3) If the stop criterion is not satisfied, set $n := n + 1$ *and go to the step (2).*

Remark 4.2. *For the first subproblem (4.2a), we can use the Gauss-Seidel method as shown in [28] to get the solution. However, in this paper, we use the following strategy:*

$$u_{i,j}^n = \frac{\theta f_{i,j} + \mu_1 \mathrm{div}(v_{i,j}^{n-1} - d_{1,i,j}^{n-1}) + 4\mu_1 u_{i,j}^{n-1} - \mu_2 \mathrm{div}^2(z_{i,j}^{n-1} - d_{2,i,j}^{n-1}) + 28\mu_2 u_{i,j}^{n-1}}{\theta + 4\mu_1 + 28\mu_2}, \tag{4.3}$$

where some information of operators Δ *and* Δ^2 *related to* u *is used. The formulas (4.2b) and (4.2c) of Algorithm 4.1 can be easily deduced from*

$$\min_v |(1-g)v|_{L^1} + \frac{\mu_1}{2} \|v - \nabla u^n - d_1^{n-1}\|_{L^2}^2$$

and

$$\min_z |gv|_{L^1} + \frac{\mu_2}{2} \|z - \nabla^2 u^n - d_2^{n-1}\|_{L^2}^2.$$

Furthermore, following form Theorem 3.1, we can also deduce that the sequence $\{u^n\}$ *generated by Algorithm 4.1 converges to the solution of (1.7).*

Algorithm 4.2. *Proximal point method (PPM) to solve (1.7).*

(1) Choose the original $d_1^0 = \boldsymbol{0} \in S$, $d_2^0 = \boldsymbol{0} \in Z$ *and* $u^0 = f$. *Set* $\mu_1, \mu_2 > 0$ *and* $n = 1$;

(2) Compute (d_1^n, d_2^n, u^n) *by*

$$\begin{cases} d_1^n = \frac{\nabla u^n + d_1^{n-1}}{|\nabla u^n + d_1^{n-1}|_{L^1}} \cdot \min(|\nabla u^n + d_1^{n-1}|_{L^1}, 1), \\ d_2^n = \frac{\nabla^2 u^n + d_2^{n-1}}{|\nabla^2 u^n + d_2^{n-1}|_{L^1}} \cdot \min(|\nabla^2 u^n + d_2^{n-1}|_{L^1}, 1), \\ u^n = f - \frac{\mu_1}{\theta}(1-g)\mathrm{div} d_1^n + \frac{\mu_2}{\theta} g \mathrm{div}^2 d_2^n; \end{cases}$$

(3) If the stop criterion is not satisfied, set $n := n + 1$ and go to the step (2).

For Algorithm 4.2, based on the relations in (4.1) and Theorem 3.2, we have the following result.

Theorem 4.1. *If $\mu_1 \in (0, \frac{1}{8\theta})$ and $\mu_2 \in (0, \frac{1}{64\theta})$, then the sequence $\{u^n\}$ generated by Algorithm 4.2 converges to the solution of (1.7).*

Remark 4.3. *For the above two algorithms, we can also set g as a constant between 0 and 1. In fact, it is easy to find that the algorithms correspond to solving the ROF model or the LLT model respectively when $g = 0$ or $g = 1$. At this time, the iteration strategy can be simplified as*

$$u_{i,j}^n = \frac{\theta f_{i,j} + \mu_1 \mathrm{div}(v_{i,j}^{n-1} - d_{1,i,j}^{n-1}) + 4\mu_1 u_{i,j}^{n-1}}{\theta + 4\mu_1}$$

and

$$u_{i,j}^n = \frac{\theta f_{i,j} - \mu_2 \mathrm{div}^2(z_{i,j}^{n-1} - d_{2,i,j}^{n-1}) + 28\mu_2 u_{i,j}^{n-1}}{\theta + 28\mu_2}$$

for these two models, respectively. Furthermore, when $g \in (0, 1)$, these two algorithms correspond to solve the model which is the convex combination of the ROF model and the LLT model.

Examples 4.1. *In this example, we compare the alternating direction method of multipliers (ADMM) with the proximal point method (PPM) for solving the ROF model (1.4), the LLT model (1.6) and the hybrid model (1.7). The original images with three different sizes shown in Figure 1 are added the Gaussian white noise with the standard deviation $\sigma = 15.3$. Iterations were terminated when the stop condition $\frac{\|u^{n+1}-u^n\|_{\ell^2}}{\|u^n\|_{\ell^2}} \le \varepsilon$ are met. The related results are arranged in Table 1, 2 and 3. It is easy to find from Table 1 that the PPM is faster than the ADMM. Especially, the average CPU time of the PPM compared with that of the ADMM can save about 50% for the ROF model and the LLT model. It saves about 40% for the hybrid model.*

$g = 0$	**The ROF Model**						
Size	Stopping Conditions ε	ADMM			PPM		
		Time(s)	Ite.	SNR	Time(s)	Ite.	SNR
128×128	1.0×10^{-4}	0.2184	86	24.7949	0.1248	83	24.7043
256×256	1.0×10^{-4}	0.9204	77	16.2934	0.2652	38	16.3540
512×512	1.0×10^{-4}	4.3368	64	15.7146	1.9656	53	15.9353
$g = 1$	**The LLT Model**						
Size	Stopping Conditions ε	ADMM			PPM		
		Time(s)	Ite.	SNR	Time(s)	Ite.	SNR
128×128	1.0×10^{-4}	0.4368	60	24.5688	0.3432	80	25.0287
256×256	1.0×10^{-4}	1.7004	55	16.9065	0.9360	53	16.9083
512×512	1.0×10^{-4}	15.4441	55	15.9432	7.2384	50	15.9512
$g \in (0, 1)$	**The Hybrid Model**						
Size	Stopping Conditions ε	ADMM			PPM		
		Time(s)	Ite.	SNR	Time(s)	Ite.	SNR
128×128	1.0×10^{-4}	0.7176	69	25.7224	0.5304	70	25.4982
256×256	1.0×10^{-4}	2.5584	55	16.9699	1.4664	52	16.9701
512×512	1.0×10^{-4}	19.6561	56	15.9503	9.3445	50	15.9512

Table 1: The related results in Example 1.

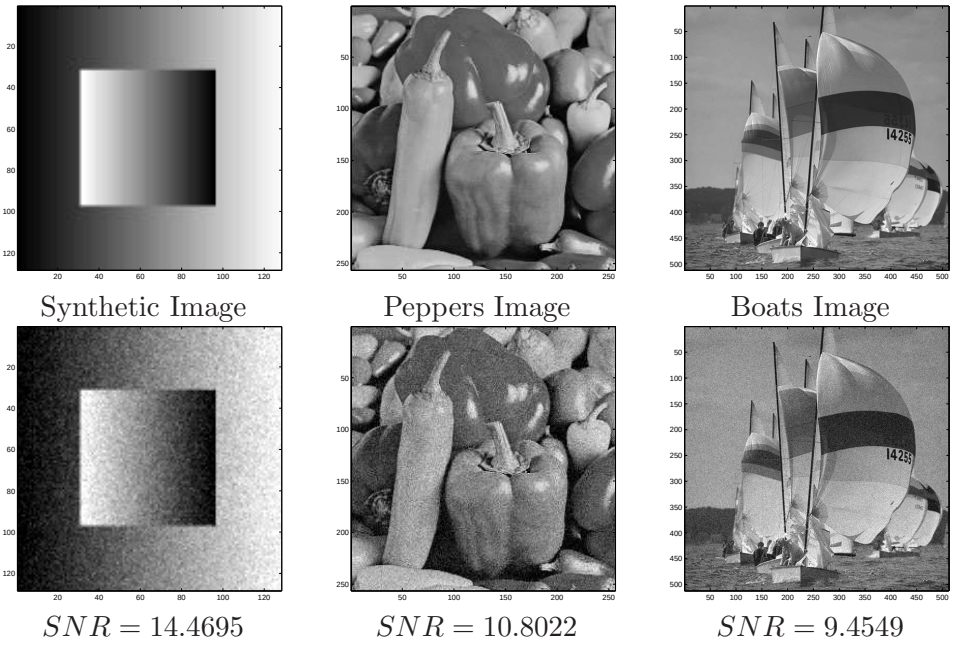

Figure 1: The original images and the noisy images with three different sizes.

Examples 4.2. *In this example, the noisy image is added the Gaussian white noisy with the standard deviation* $\sigma = 12$. *The algorithms will be stopped after 100 iterations. We compare the results generated by the ROF model, the LLT model, the convex combination of the ROF model and the hybrid model. As we can see from Table 2, the hybrid model get the lowest* MSE *and the biggest* SNR, *these imply that the hybrid model can give the best restored image. On the other hand, it is easy to find that the ROF model makes staircasing effect appear and the LLT model leads to edge blurring. In fact, they are based on the fact that the restored model by the ROF model is piecewise constant on large areas and the LLT model as a higher model damps oscillations much faster in the region of edges. For the convex combined model and the hybrid model, they can efficiently suppress these two drawbacks. Furthermore, the hybrid model is more efficient than the convex combined model, it is because that the hybrid model uses the edge detector function which can efficiently coordinate edge information. It should be noticed that here we use the Chambolle's strategy [12] to solve the convex combined model so that it is slower than the strategy by using the PPM to solve the hybrid model. To focus on these facts, we present the some zoomed-in local results and select a slice of the images that meets contours and the smooth regions shown in Figure 2 and 3.*

Model	R. P.	Time (s)	SNR	MSE
ROF	4.5	0.8268	17.7677	44.0400
LLT	3.0	2.0904	17.9998	42.7826
Convex	3.5	2.6832	18.2399	39.7756
Hybrid	4.5	2.5272	18.3694	39.1447

Table 2: The related data in Example 2. (Here R.P. is the regularization parameter.)

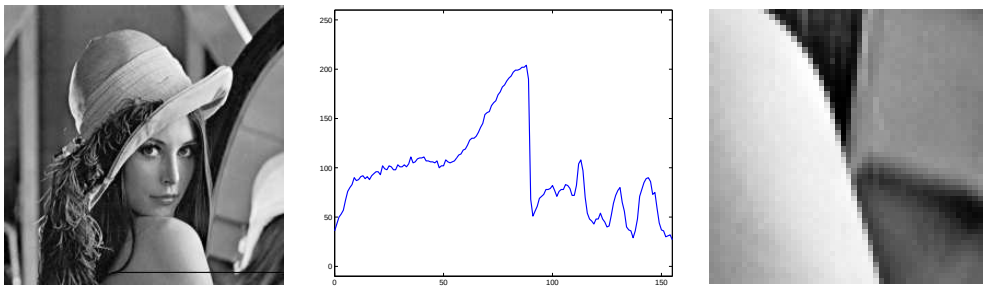

(a)Original Image Slice Local Zomming

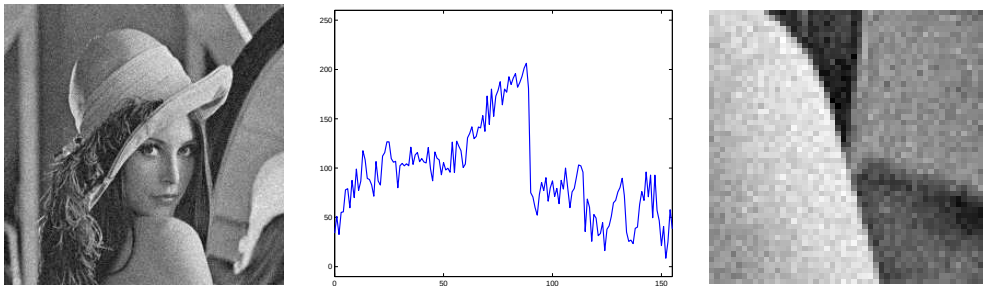

(b)Noisy Image Slice Local Zomming

Figure 2: The original and the noisy image.

4.2. Other applications

In this subsection, we extend the hybrid model to other classes of restoration problems. As we can see in subsection 4.1, the hybrid model has some advantages compared with the ROF model and the LLT model. Since the PPM is faster and more efficient than the ADMM, we only employ the PPM to solve the related image restoration model. Now we first consider the following iteration strategy

$$\begin{cases} z^n = \mathcal{F}(u^n) =: \arg\min\limits_z \dfrac{\beta}{2}\|u^n - z\|_{L^2}^2 + h(z), & \text{(4.4a)} \\ u^{n+1} = \mathcal{G}(z^n) := \arg\min\limits_u \underbrace{\dfrac{\beta}{2}\|u - z^n\|_{L^2}^2 + \int_\Omega |(1-g)\nabla u|\mathrm{d}x + \int_\Omega |g\nabla^2 u|\mathrm{d}x}_{\mathcal{D}(u)}, & \text{(4.4b)} \end{cases}$$

where $h(z) \in C^1(\Omega)$. It is easy to find that the minimization problem $\mathcal{D}(u)$ in (4.4b) is coercive and strictly convex, so the subproblem (4.4b) has a unique solution. Based on Lemma 2.4 in [21], we also deduce that the operator $\mathcal{G}$ is $\frac{1}{2}-$averaged nonexpansive.

Theorem 4.2. *Assume that the functional*

$$\mathcal{M}(u,z) = \frac{\beta}{2}\|u - z\|_{L^2}^2 + h(z) + \int_\Omega |(1-g)\nabla u|\mathrm{d}x + \int_\Omega |g\nabla^2 u|\mathrm{d}x$$

is convex, coercive and bounded below, then the sequence $\{(u^n, z^n)\}$ generated by (4.4) converges to a point (u^*, z^*). Furthermore, when $u^* = z^*$, u^* is the solution of

$$\min_u h(u) + \int_\Omega |(1-g)\nabla u|\mathrm{d}x + \int_\Omega |g\nabla^2 u|\mathrm{d}x. \tag{4.5}$$

Proof. From the assumption, the functional $\mathcal{M}(u,z)$ has at least solution denoted by $(\bar{u}, \bar{z})$, which

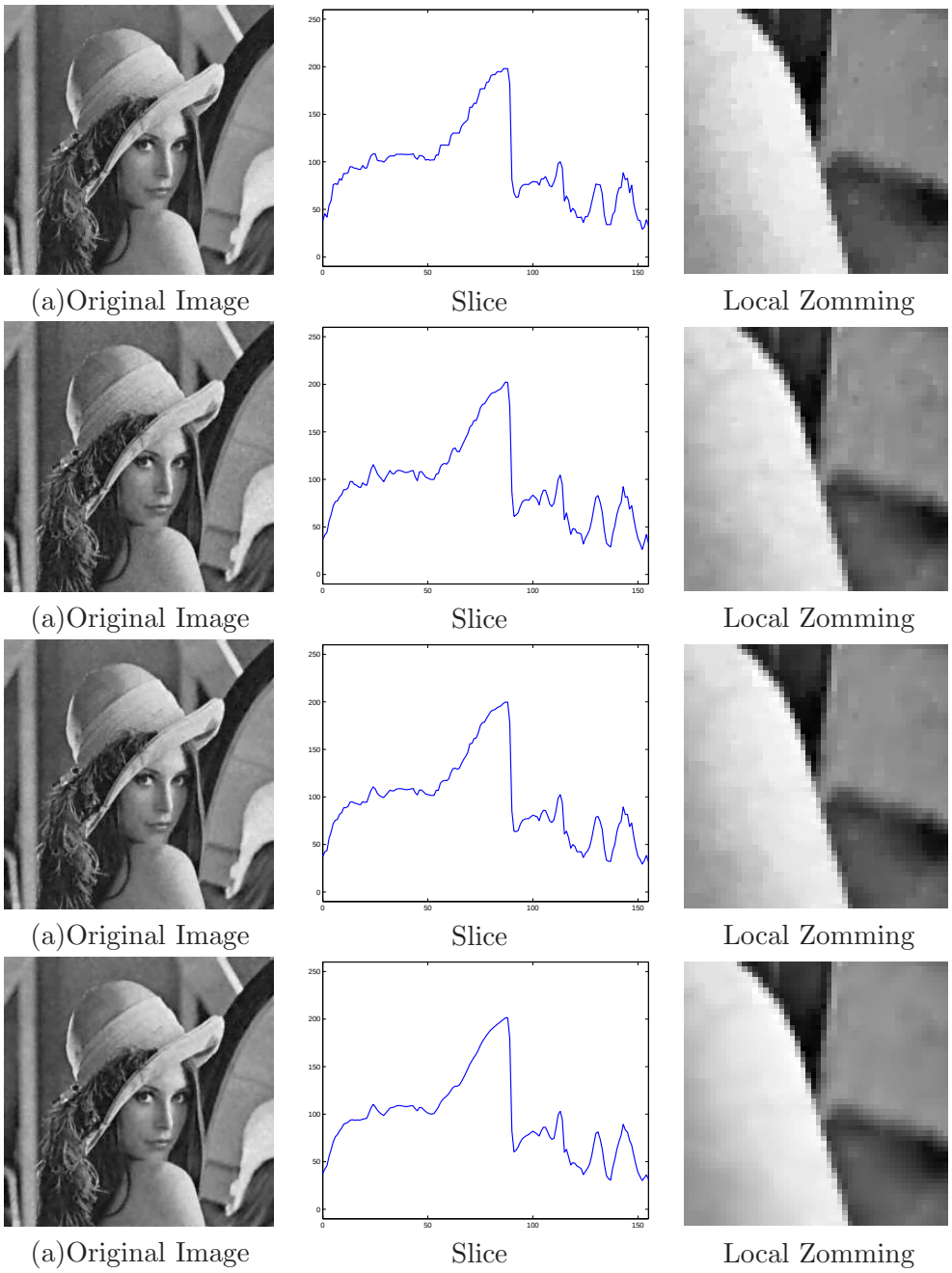

Figure 3: The related restored images.

implies that $(\bar{u}, \bar{z})$ satisfies

$$\begin{cases} \bar{z} = \mathcal{F}(\bar{u}), \\ \bar{u} = \mathcal{G}(\bar{z}). \end{cases}$$

That is to say that $\bar{u}$ is a fixed point of the operator $\mathcal{G} \circ \mathcal{F}$.

Now we show that the sequence $\{u^n\}$ generated by (4.4) converges to this fixed point $\bar{u}$. In fact, based on the nonexpansive operators $\mathcal{F}$ and G, for the sequence $\{u^n\}$ we can get

$$\|u^{n+1} - \bar{u}\|_{L^2} = \|\mathcal{F} \circ \mathcal{G}(u^n) - \mathcal{F} \circ \mathcal{G}(\bar{u})\|_{L^2} \leq \|u^n - \bar{u}\|_{L^2}.$$

This implies that the positive sequence $\{\|u^n - \bar{u}\|_{L^2}\}$ is monotonically decreasing. So we can find a subsequence $\{u^{n_k}\}$ from $\{u^n\}$ converging to a limit point u^* as $n \to \infty$. Form the continuous of $\mathcal{F}$ and $\mathcal{G}$, we then have

$$\|u^* - \bar{u}\|_{L^2} = \|\mathcal{F} \circ \mathcal{G}(u^*) - \bar{u}\|_{L^2}.$$

Furthermore, we can get $\bar{u} = u^*$ based on the uniqueness of the fixed point. Thus, (u^*, z^*) is the solution of (4.4), here z^* corresponds to u^*. Set $J(u) = \int_\Omega |(1-g)\nabla u| \mathrm{d}x + \int_\Omega |g\nabla^2 u| \mathrm{d}x$, we can get

$$\begin{cases} 0 = \beta(z^* - u^*) + h'(z^*), \\ 0 \in \beta(u^* - z^*) + \partial J(u^*), \end{cases}$$

which implies that

$$h'(z^*) + \partial J(u^*) = 0.$$

Then, when $u^* = z^*$, u^* is the solution of (4.5). □

Remark 4.4. *It should be noticed that the following three models satisfy the conditions of Theorem 4.2, so we can use the strategy (4.4) to solve these models.*

4.2.1. Image deblurring

Now we apply the hybrid model to the image deblurring problems with the following formula

$$\min_u \frac{\lambda}{2}\|Ku - u_0\|_{L^2}^2 + |u|_{BV_{(1-g)}} + |u|_{BV_g^2}. \tag{4.6}$$

Because of the compactness, the blurring operator K is not continuously invertible, which implies that we can not directly use the proximal method to solve minimization problem (4.6). However, based on the penalty method [9], we can transform the problem (4.6) to solve the following problem

$$\begin{cases} z^n = (\mu\lambda K^T K + I)^{-1}(\mu\lambda K^T f + u^n), & \text{(4.7a)} \\ u^{n+1} := \arg\min_u \dfrac{1}{2\mu}\|u - z^n\|_{L^2}^2 + \displaystyle\int_\Omega |(1-g)\nabla u| \mathrm{d}x + \int_\Omega |g\nabla^2 u| \mathrm{d}x. & \text{(4.7b)} \end{cases}$$

The key of (4.7) is to separate the blurring operator K from the original problem (4.6) so that we can avoid the ill-posed operator K. Furthermore, it is obvious that the problem (4.7b) satisfies Lemma 4.1, so we can use the proximal method to solve it.

Examples 4.3. *In this experiment, we use the image Lena, which are blurred with a Gaussian kernel of "hsize=3" and added the Gaussian white noise with the standard deviation $\sigma = 0.02$. The related images and SNRs are arranged in Figure 4. As we can see in Example 1, the proximal method tends to be stable before 100 iterations, so here we fix the algorithm to be stopped when the iteration attains 100. It is easy to find that the hybrid model can give a better image quality than other two models. Especially, we also observe some staircasing effect in Figure 4(b) and edge blurring in Figure 4(c). However, all of drawbacks can be efficiently suppressed in Figure 4(d).*



(a)Original Image (b)The ROF Model

(c)The LLT Model (d)The Hybrid Model

Figure 4: The related SNRs. (a)11.2166; (b)14.3378; (c)14.4778; (d)14.5118.

4.2.2. Image inpainting

Here we consider to use the hybrid model for the image inpainting problem with the following form:

$$\min_u \frac{\bar{\lambda}}{2}\|u-u_0\|^2_{L^2(\Omega\setminus D)} + |u|_{BV_{(1-g)}(\Omega)} + |u|_{BV^2_g(\Omega)},$$

where D is the inpainting domain and $\bar{\lambda}$ satisfies

$$\bar{\lambda} = \begin{cases} \lambda, & \text{if } u \in \Omega \setminus D, \\ 0, & \text{if } u \in D. \end{cases}$$

If we introduce an auxiliary variable z, based on the penalty method [9] again, then the solution of the problem (4.7) can be approximated by solving the following problem

$$\begin{cases} u^n := \dfrac{z^n + \bar{\lambda}\mu u_0}{1+\bar{\lambda}\mu}, & \text{(4.8a)} \\ z^{n+1} := \arg\min\limits_z \dfrac{1}{2\mu}\|z-u^n\|^2_{L^2(\Omega)} + \displaystyle\int_\Omega |(1-g)\nabla z|\mathrm{d}x + \int_\Omega |g\nabla^2 z|\mathrm{d}x. & \text{(4.8b)} \end{cases}$$

Examples 4.4. *In this example, we show the results of real image inpainting in Figure 5 and 6. We consider to use these three models to restore images shown in Figure 5 (c) and (d), which are respectively contaminated by the mask image and the noise with the standard deviation $\sigma = 12$. The parameters of these three models are chosen for getting betters restored images and the*

algorithms will be stopped after 500 iterations. It is obvious that these three models can efficiently restore the original deteriorated images. However, there are much more inappropriate information restored by the ROF model than the LLT model and the hybrid model. These advantages is based on the fact that fourth-order linear (the LLT model and the hybrid model) damps oscillations much faster than second-order diffusion (the ROF model). Especially, these unsuitable effects can be easily seen from the local zooming images in Figure 6 and 7. Furthermore, the restored image by the hybrid model looks more natural images than the LLT model.

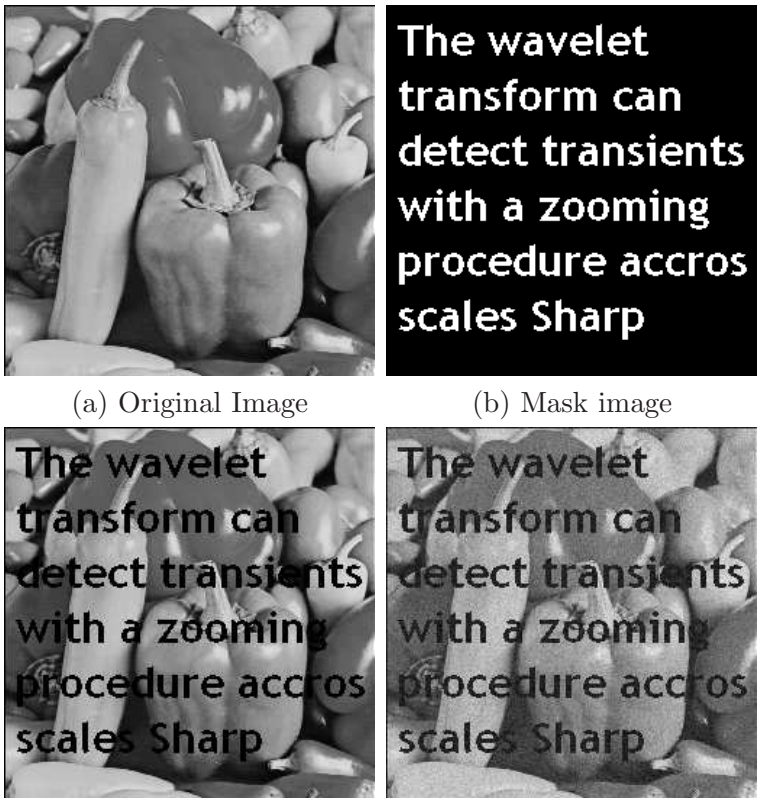

(a) Original Image (b) Mask image

(c) Painting image (d) Noisy image

Figure 5: The related images in Example 4.

Model	Image (c) in Figure 5			Image (d) in Figure 5		
	λ	μ	SNR	λ	μ	SNR
ROF	220	0.005	18.5533	32	0.008	15.4055
LLT	150	0.005	16.2934	60	0.005	16.4336
Hybrid	220	0.005	20.2713	70	0.0025	16.6034

Table 3: The related results in Example 1.

4.2.3. Image denoising for the multiplicative noise

Based on the hybrid model (1.7), the multiplicative noise model (1.5) can be naturally ex-


(a) The ROF Model


(b) The LLT Model


(c) The Hybrid Model


(a1) Local Zooming


(b1) Local Zooming


(c1) Local Zooming

Figure 6: The related restored images corresponding to the painting image.


(a) The ROF Model


(b) The LLT Model


(c) The Hybrid Model


(a1) Local Zooming


(b1) Local Zooming


(c1) Local Zooming

Figure 7: The related restored images corresponding to the noisy image.

tended to the following minimization

$$\min_z \alpha \int_\Omega \Big(z + fe^{-z}\Big)\mathrm{d}x + \int_\Omega |(1-g)\nabla z|\mathrm{dx} + \int_\Omega |g\nabla^2 z|\mathrm{d}x. \tag{4.9}$$

It is obvious that the problem (4.9) can be approximated by

$$\begin{cases} u^n := \arg\min_u \dfrac{1}{2\mu}\|z^n - u\|_{L^2}^2 + \alpha \displaystyle\int_\Omega \left(u + fe^{-u}\right)\mathrm{d}x, & \text{(4.10a)} \\ z^{n+1} := \arg\min_z \dfrac{1}{2\mu}\|z - u^n\|_{L^2}^2 + \displaystyle\int_\Omega |(1-g)\nabla z|\mathrm{d}x + \int_\Omega |g\nabla^2 z|\mathrm{d}x. & \text{(4.10b)} \end{cases}$$

For the first subproblem (4.10a), its solution u^n can be approximately obtained by using the Newton method to solve the following nonlinear equation

$$\mu(u - z^n) + \alpha(1 - fe^{-u}) = 0. \tag{4.11}$$

Examples 4.5. *In this example, we restore the multiplicative noisy image. The noisy Lena image shown in Figure 7 is contaminated by the Gamma noise (L=33) with mean one, which probability density function $p(u)$ is given by*

$$p(u) = \begin{cases} \frac{L^L u^{L-1}}{\Gamma(L)} e^{-Lu}, & \text{if } u > 0, \\ 0, & \text{if } u \le 0, \end{cases}$$

where L is an integer and $\Gamma(\cdot)$ is a Gamma function. Based on the iteration formula (4.10), we should notice that there include two interior iterations. For employing the Newton method to solve the problem (4.11), we set the stepsize $t = 1$ and the Newton method will be stopped when $\frac{\|u^{n+1}-u^n\|_{\ell^2}}{\|u^n\|_{\ell^2}} \le 1.0 \times 10^{-5}$. For solving the second subproblem (4.10b), we set the fixed iterations with 40. In fact for using the PPM to solve the ROF model, the LLT model and the hybrid model, the solutions of these models will be tend to the steady. The outer iteration will be stopped after 200 iterations. The related restored images are shown in Figure 7, it is easy to find that the hybrid model gives a better restored image than two other models.

5. Concluding Remarks

In this paper, based on the edge detector function, we proposed a hybrid model to overcome some drawbacks of the ROF model and the LLT model. Following the augmented Lagrangian method, we can employ the alternating direction method (ADMM) of multipliers to solve this hybrid model. In this paper, we mainly proposed the proximal point method (PPM) to solve this model due to the fact that the PPM unnecessarily solves a PDE compared with the ADMM so that it is more effective than the ADMM. The convergence of the proposed method was also given. However, the convergence rate of the proposed method is only $O(1/k^2)$, so our future work is to improve our method with convergence rate $O(1/k^2)$ based on the some strategies in [7, 37]

Acknowledgements

The first author would like to thank the Mathematical Imaging and Vision Group in Division of Mathematical Sciences at Nanyang Technological University in Singapore for the hospitality during the visit. This research is supported by Singapore MOE Grant T207B2202, Singapore NRF2007IDM-IDM002-010, the NNSF of China (No. 60835004, 60872129).

References

[1] M. Afonso, J. Bioucas-Dias, and M. Figueiredo. Image restoration with compound regularization using a Bregman iterative algorithm. Signal Processing with Adaptive Sparse Structured Representations, 2009.



(a) The Noisy Image (b) The ROF Model



(c) The LLT Model (d) The Hybrid Model



(b1) The ROF Model (c1) The LLT Model (d1) The Hybrid Model

Figure 8: The related images and the local zooming images. SNRs: (a)9.2017; (b)15.6059; (c)15.1754; (d)16.0546.

[2] L. Ambrosio, N. Fusco, D. Pallara. Functions of Bounded Variation and Free Discontinuity Problems. Oxford University Press, 2000.

[3] H. Attouch, G. Buttazzo, G. Michaille. Variational Analysis in Sobolev and BV Spaces: Applications to PDEs and Optimization. SIAM, 2006.

[4] G. Aubert and J. Aujol. A variational approach to removing multiplicative noise. SIAM Journal on Applied Mathematics, 68(4)(2008), 925-946.

[5] G. Aubert and P. Kornprobst. Mathematical Problems in Image Processing: Partial Differential Equations and the Calculus of Variations. Springer-Verlag, New York, 2002.

[6] J. Aubin and H. Frankowska. Set-Valued Analysis. Springer, 1990.

[7] A. Beck and M. Teboulle. A fast iterative shrinkage-thresholding algorithm for linear inverse problems. SIAM Imaging Sciences, 2(1)(2009), 183-202.

[8] A. Bermudez and C. Moreno. Duality methods for solving variational inequalities. Computers & Mathematics with Applications, 7(1)(1981), 43-58.
[9] D. Bertsekas. Constrained Optimization and Lagrange Multiplier Methods. Athena Scientific, 1996.
[10] M. Burger, K. Frick, S. Osher, and O. Scherzer. Inverse total variation flow. Multiscale Modeling Simulation, 6(2)(2007), 366-395.
[11] J. Cai, S. Osher, and Z. Shen. Split Bregman methods and frame based image restoration. Multiscale Modeling Simulation, 8(2)(2009), 337-369.
[12] A. Chambolle. An algorithm for total variation minimization and applications. Journal of Mathematical Imaging and Vision, 20(1-2)(2004), 89-97.
[13] A. Chambolle. Total variation minimization and a class of binary MRF models. In:EMMCVPR, 05(2005), 136-152.
[14] A. Chambolle and T. Pock. A first-order primal-dual algorithm for convex problems with applications to imaging. Journal of Mathematical Imaging and Vision, 40(1)(2011), 120-145.
[15] T. Chan, A. Marquina, and P. Mulet. High-order total variation-based image restoration. SIAM Journal on Scientific Computing, 22(2)(2000), 503-516.
[16] T. Chan and J. Shen. Image Processing and Analysis-Variational, PDE, Wavelet, and Stochastic Methods. SIAM , Philadelphia, 2005.
[17] T. Chan and J. Shen. On the role of the BV image model in image restoration. Communications on Pure and Applied Mathematics. 58(5)(2005), 579-619.
[18] T . Chan, J. Shen, and H. Zhou. Total variation wavelet inpainting. Journal of Mathematical Imaging and Vision, 25(1)(2006), 107-125.
[19] B. Charles. Applied Iterative Methods. A K Peters, Ltd, 2007.
[20] K. Chen and X. Tai. A nonlinear multigrid method for total variation minimization from image restoration. Journal of Scientific Computing, 33(2)(2007), 115-138.
[21] P. Combettes and V. Wajs. Signal recovery by proximal forward-backward splitting. Multiscale Modeling Simulation, 4(4)(2005), 1168-1200.
[22] H. Engl, M Hanke and A. Neubauer. Regularization of Inverse Problems. Kluwer Academic Publishers, 1996.
[23] E. Esser. Applications of the Lagrangian-based alternating direction methods and connections to split Bregman. UCLA Report 2009-31.
[24] E. Esser, X. Q. Zhang, and T. Chan. A general framework for a class of first order primal-dual algorithms for TV. SIAM Journal on Imaging Sciences, 3(4)(2010), 1015-1046.
[25] L. Evans, R. Gariepy. Measure Theory and Fine Properties of Functions. Boca Raton: CRC. press, 1992.
[26] R. Gao, J. Song, and X. Tai. Image zooming algorithm based on partial differential equations. International Journal of Numerical Analysis and Modeling, 6(2)(2009), 284- 292.
[27] D. Goldfarb and W. Yin. Second-order cone programming methods for total variation based image restoration. SIAM Journal on Scientific Computing, 27(2)(2005), 622-645.
[28] T. Goldstein and S. Osher. The split Bregman for L^1 regularized problems. SIAM Journal on Imaging Sciences, 2(2)(2009), 323-343.
[29] Y. Huang, M. Ng, and Y. Wen. A new total variation method for multiplicative noise removal. SIAM Journal on Imaging Sciences, 2(1)(2009), 20-40.
[30] I. Ekeland and R. Teman. Convex Analysis and Variational Problems. North-Holland, Amsterdam, 1976.
[31] F. Li, C. Shen, J. Fan, and C. Shen. Image restoration combining a total variational filter and a fourth-order filter. Journal of Visual Communication and Image Representation. 18(4)(2007), 322-30.

[32] M. Lysaker, A. Lundervold, and X. Tai. Noise removal using fourth-order partial differential equation with applications to medical magnetic resonance images in space and time. IEEE Transactions on Image Processing, 12(12)(2003), 1579-1590.

[33] A. Marquina and S. Osher. Image super-resolution by TV-regularization and Bregman iteration. Journal of Scientific Computing, 37(3)(2008), 367-382.

[34] Y. Meyer. Oscillating Patterns in Image Processing and Nonlinear Evolution Equations. University Lecture Series, AMS, 2001.

[35] A. Micchelli, L. X. Shen, and Y. S. Xu. Proximity algorithms for image models: denoising. Inverse Problems 27(4)(2011), print.

[36] A. Montillo, J. Udupa, L. Axel, and D. Metaxas. Interaction between noise suppression and inhomogeneity correction in MRI. Proceedings of SPIE, 5032(2003), 1025-1036.

[37] Y. Nesterov. A method for unconstrained convex minimization problem with the rate of convergence $O(\frac{1}{k^2})$. Soviet Mathematics Doklady, 27(2)(1983), 372-376.

[38] N. Paragios, Y. Chen, and O. Faugeras. The Handbook of Mathematical Models in Computer Vision. Springer-Verlag, New York, 2005.

[39] A. Pazy. On the asymptotic behavior of iterates of nonexpansive mappings in Hilbert space. Israel Journal of Mathematics, 26(2)(1977), 197-204.

[40] L. Rudin and S. Osher. Total variation based image restoration with free local constraints. IEEE International Conference on Image Processing. 1(13-16)(1994), 31-35.

[41] L. Rudin, P. Lions, and S. Osher. Multiplicative denoising and deblurring: theory and algorithms. In Geometric Level Set Methods in Imaging, Vision, and Graphics, (2003), 103-120.

[42] L. Rudin, S. Osher, and E. Fatemi. Nonlinear total variation based noise removal algorithms. Physica D, 60(1992), 259-268.

[43] O. Scherzer. Denoising with higher order derivatives of bounded variation and an application to parameter estimation. Computing, 60(1)(1998), 1-27.

[44] S. Setzer. Split Bregman algorithm, Douglas-Rachford splitting and frame shrinkage. In:SSVMCV, 5567(2009), 464-476.

[45] X. C. Tai and C. Wu. Augmented Lagrangian method, dual methods and split Bregman iteration for ROF model. In:SSVMCV, 5567(2009), 502-513.

[46] R. Wagner, S. Smith, J. Sandrik, and H. Lopez. Statistics of speckle in ultrasound B-scans. Transactions on Sonics Ultrasonics, 30(3)(1983), 156-163.

[47] Y. Wang, J. Yang, W. Yin, and Y. Zhang. A new alternating minimization algorithm for total variation image reconstruction. SIAM Journal on Imaging Sciences, 1(3)(2008), 248-272.

[48] Y. L. You and M. Kaveh. Fourth-order partial differential equation for noise removal. IEEE Transactions on Image Processing, 9(10)(2000), 1723-1730.

[49] M. Zhu and T. Chan. Duality-based algorithms for total-variation-regularized image restoration. Computational Optimization and Applications, 47(3)(2010), 377-400.